NANO LETTERS

Letter

pubs.acs.org/NanoLett

Selective Supramolecular Fullerene–Porphyrin Interactions and Switching in Surface-Confined C_{60}–Ce(TPP)$_2$ Dyads

Saranyan Vijayaraghavan,[†] David Écija,*[,†] Willi Auwärter,*[,†] Sushobhan Joshi,[†] Knud Seufert,[†] Ari P. Seitsonen,[‡] Kentaro Tashiro,[§] and Johannes V. Barth[†]

[†]Physik Department E20, Technische Universität München, D-85748 Garching, Germany

[‡]University of Zurich, Physikalisch-Chemisches Institut, Winterthurerstrasse 190, CH-8057 Zurich, Switzerland

[§]International Center for Materials Nanoarchitectonics, National Institute for Materials Science (NIMS) 1-1 Namiki, Tsukuba 305-0044, Japan

Supporting Information

ABSTRACT: The control of organic molecules, supramolecular complexes and donor–acceptor systems at interfaces is a key issue in the development of novel hybrid architectures for regulation of charge-carrier transport pathways in nanoelectronics or organic photovoltaics. However, at present little is known regarding the intricate features of stacked molecular nanostructures stabilized by noncovalent interactions. Here we explore at the single molecule level the geometry and electronic properties of model donor–acceptor dyads stabilized by van der Waals interactions on a single crystal Ag(111) support. Our combined scanning tunneling microscopy/spectroscopy (STM/STS) and first-principles computational modeling study reveals site-selective positioning of C_{60} molecules on Ce(TPP)$_2$ porphyrin double-decker arrays with the fullerene centered on the π-system of the top bowl-shaped tetrapyrrole macrocycle. Three specific orientations of the C_{60} cage in the van der Waals complex are identified that can be reversibly switched by STM manipulation protocols. Each configuration presents a distinct conductivity, which accounts for a tristable molecular switch and the tunability of the intradyad coupling. In addition, STS data evidence electronic decoupling of the hovering C_{60} units from the metal substrate, a prerequisite for photophysical applications.

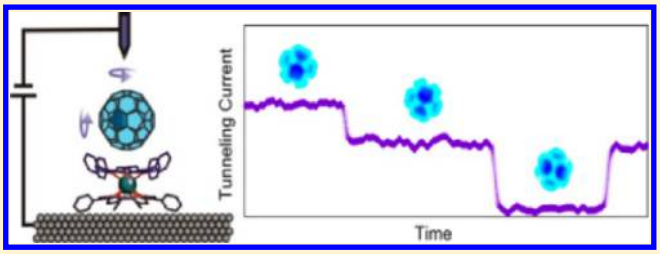

KEYWORDS: *Self-assembly, scanning tunneling microscopy, scanning tunneling spectroscopy, molecular switches, donor/acceptor dyads*

Molecular donor–acceptor (D–A) systems are considered to be crucial ingredients to construct novel organic solar cells based on heterojunction interfaces[1−3] that serve to dissociate strongly bound photogenerated excitons.[4,5] Herein, research efforts focus both on the combination of different D–A materials and the intermolecular coupling mechanisms aiming at the maximization of the power conversion efficiency of the device.[6] Specifically, fullerene–porphyrin architectures attract considerable interest given their remarkable photoactive, structural, and magnetic properties.[7,8] Fullerenes present extraordinary electron-accepting characteristics, promoting ultrafast charge separation and exhibiting very slow charge recombination characteristics.[9] On the other hand, as key players in natural photosynthesis, porphyrins are ideal light harvesting units to be combined with electron acceptors as fullerenes. Recently, sandwich-type porphyrin and related tetrapyrrole complexes incorporating large central rare-earth ions have attracted widespread attention.[10−14] In particular, their unique electronic and optical properties include tunable broadband absorption, large exciton delocalization length, and ultrafast energy transfer between the macrocycles, which make these complexes as promising donors for photovoltaic devices.[15,16] Accordingly, recent articles report successful photovoltaic cells with increased power conversion efficiency based on such complexes.[17−20] In order to improve the performance of these devices it is of paramount importance to thoroughly characterize the D–A interface, where the decisive exciton dissociation takes place.[6]

Beyond being prototypes for D–A heterojunctions in organic photovoltaics, surface-confined dyads (bimolecular units) provide significant potential for organic light-emitting diodes, molecular switches, or molecular machinery. The binding characteristics and the inherent electronic and mechanical properties of such bimolecular nanostructures can be controlled by appropriately choosing the type of intermolecular interactions. Especially interesting are dyads where molecular recognition and stabilization occurs via weak van der Waals interactions, thus preserving the main electronic structure of the components and potentially permitting the molecular manipulation of the constituents. Herein, a particularly favorable situation is encountered with fullerene–porphyrin systems, where close intermolecular contacts and selective

Received: April 24, 2012
Revised: June 22, 2012

   dx.doi.org/10.1021/nl301534p | *Nano Lett.* XXXX, XXX, XXX–XXX

supramolecular interactions prevail,[21−23] however, to date only limited progress was made regarding the realization of related nanoscale arrangements amenable to single molecule investigations. For an in-depth understanding of the physicochemical principles of such systems, a thorough characterization of the geometric, mechanical, and electronic properties of the dyad and the D−A interface is mandatory.

To this end, we construct C_{60}−$Ce(TPP)_2$ dyads via self-assembly on Ag(111) as a model system to study the coordination of a promising donor ($Ce(TPP)_2$)[15,16] and a well-established acceptor unit (C_{60}).[24] This approach is advantageous as the size and limited thermal stability of covalently linked dyads[25] generally prevents a direct sublimation of the entire complex onto surfaces. In addition, studies of D−A dyads assembled by noncovalent interactions at solid−liquid interfaces lack the resolution to elucidate the nature of the intermolecular interactions involved and, thus, cannot address the essential details of the D−A interface.[26] In particular, by combining scanning tunneling microscopy (STM) and scanning tunneling spectroscopy (STS) experiments, we report the site-selective adsorption, electronic characterization, molecular orientation, and controlled manipulation of C_{60} molecules on regular arrays of $Ce(TPP)_2$ double-decker complexes adsorbed on a Ag(111) single crystal support. The in situ formed dyads exhibit a predominant face-to-face geometry between a porphyrin derivative and fullerenes which, despite considerable efforts, was not achieved previously at interfaces under ultrahigh vacuum conditions.[27,28] This highly controlled environment allows us to characterize the geometric, electronic, and mechanical properties of the system in exquisite detail. Our findings thus present a new approach toward surface-confined porphyrin−fullerene D−A dyads and the intricate supramolecular interactions involved, which go beyond commonly employed noncovalent bonding schemes.[29]

$Ce(TPP)_2$ arrays are assembled on a Ag(111) substrate via direct sublimation or an in situ synthesis procedure.[14] Figure 1a shows a double-decker array prepared by depositing 0.2 monolayer (ML) of $Ce(TPP)_2$ and subsequent annealing to 230 °C. As detailed in ref 14, the double deckers self-assemble into a dense packed phase. These islands feature a square unit cell that includes two $Ce(TPP)_2$ entities characterized by a different orientation of the top porphyrin (labeled α and β) and an intermolecular distance of 13.9 ± 0.5 Å . The structural models in Figure 1b highlight the orientations of the top porphyrins in the α (green model) and β (red model) species differing by 90°. Within the assembly, all bottom porphyrins have the same orientation and are rotated by ±45° with respect to the top porphyrin. High-resolution images (cf. Figure 1a) exhibit a two-fold symmetry of the top porphyrin macrocycle, which indicates a nonplanar deformation.[14] The reduced symmetry allows us to define a main axis of the molecule (grey lines in Figure 1b) and gives rise to the α and β orientations. An overview on the voltage-dependent appearance of $Ce(TPP)_2$ is given in the Supporting Information (cf. Figure S1). The observation of a reduced macrocycle symmetry is consistent with an X-ray diffraction analysis of $Ce(OEP)_2$ revealing a slightly distorted square antiprismatic geometry with two bowled macrocycles[30] and theoretical descriptions of $Ce(OEP)_2$ and CeP_2.[31] Indeed, our DFT-based geometry optimization of an isolated $Ce(TPP)_2$, considering the experimentally observed alignment of the macrocycles, reveals a nonplanar deformation of the porphyrins and a propeller-like

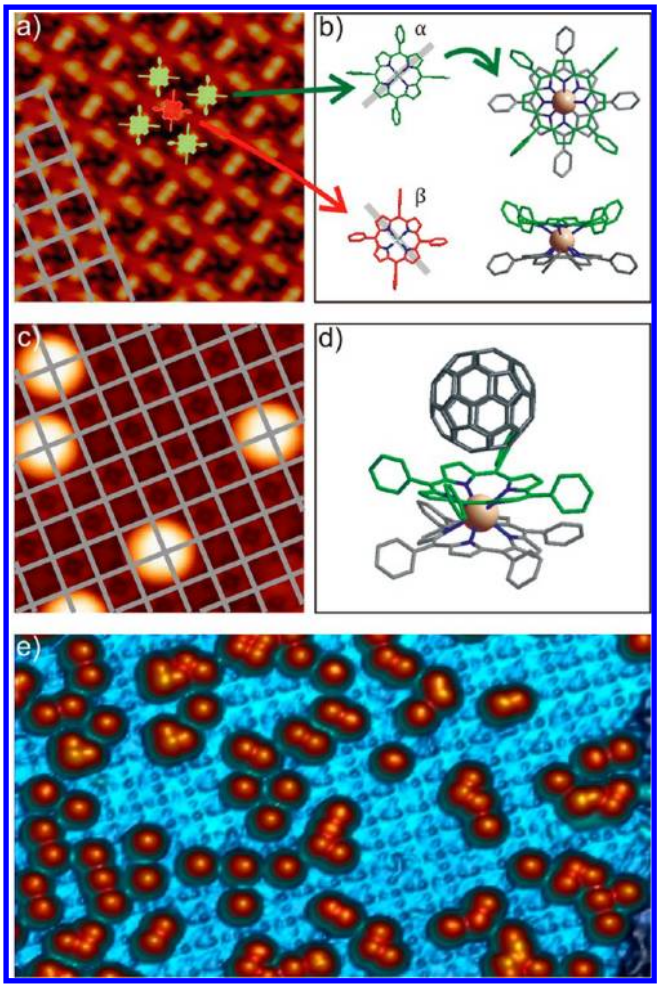

Figure 1. Site-selective adsorption of C_{60} on porphyrin double deckers. (a) STM topograph of a $Ce(TPP)_2$ array on Ag(111). The green and red models represent the two orientations (named α and β) of the nonplanar top porphyrin in the $Ce(TPP)_2$. Image size: 110.7 × 110.7 Å^2, tunneling parameters: V_b = 0.2 V, I = 0.1 nA. (b) Schematic top and side view representation of a $Ce(TPP)_2$ complex obtained from DFT calculations visualizing the bowl-shape deformation (see text for discussion). For clarity, the hydrogen atoms are not shown. The top porphyrin of the double decker is rotated ±45° with respect to the bottom one, resulting in α and β configurations. (c) Molecular recognition: the bright protrusions correspond to individual C_{60} molecules on a double-decker array, which is resolved in the background. The superimposed grid represents the centers of the $Ce(TPP)_2$ units. Image size: 110.7 × 110.7 Å^2, V_b = 1.7 V, I = 75 pA. (d) DFT-based structural model visualizing a C_{60} molecule confined on the bowl-shaped macrocycle of a double decker. (e) Pseudo 3D representation of an STM topograph at higher C_{60} coverage highlighting the influence of the square $Ce(TPP)_2$ lattice on the C_{60} positioning. Image size: 443 × 266 Å^2, V_b = 1.7 V, I = 30 pA.

arrangement of the terminal phenyl groups of the top porphyrin (cf. Figure 1b,d). In particular, the macrocycle of the top porphyrin represents a bowl-like configuration, where one opposing pair of pyrrole rings is tilted more than the other pair, giving rise to the main axis of the complex introduced above and favoring the confinement of C_{60} (vide infra), i.e., the porphyrin flexibility promotes a molecular recognition phenomenon. The Supporting Information details the asymmetries in the $Ce(TPP)_2$ structure (cf. Figure S2) and includes the atomic coordinates of the optimized $Ce(TPP)_2$ geometry.

dx.doi.org/10.1021/nl301534p | Nano Lett. XXXX, XXX, XXX−XXX

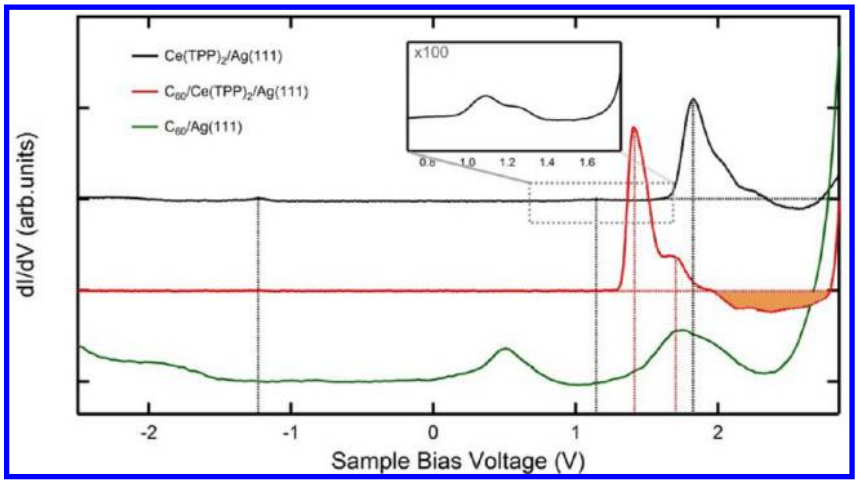

Figure 2. Electronic structure of the C_{60}–$Ce(TPP)_2$ dyad probed by STS. dI/dV traces are recorded on a single C_{60}–Ag(111) (green) and $Ce(TPP)_2$–Ag(111) (black) and a C_{60} on a $Ce(TPP)_2$–Ag(111) (red). The latter indicates a clearly reduced coupling of the fullerene to the metal substrate, showing narrow resonances, an increase of the HOMO–LUMO gap, a fingerprint of the dynamic Jahn–Teller effect, and a NDR regime shaded in orange. The inset shows the signal of the first unoccupied $Ce(TPP)_2$ resonance enlarged by a factor of 100. (Tip stabilization: V_b = 3.2 V, I = 0.15 nA, ΔV_b = 18 mV, $f_{Lock\text{-}in}$ = 969 Hz).

To assemble C_{60}–$Ce(TPP)_2$ dyads, small amounts of C_{60} were deposited on porphyrin double-decker arrays held at 120 K. Generally, we employed submonolayer $Ce(TPP)_2$ coverages enabling a direct comparison of C_{60} adsorption on bare Ag(111) and $Ce(TPP)_2$. The STM images in Figure 1c,e recorded after the deposition of C_{60} onto the precursor lattice show individual C_{60} molecules on top of the $Ce(TPP)_2$ island. An analysis of STM data exhibiting submolecular resolution allows us to identify the adsorption sites of C_{60} on $Ce(TPP)_2$ and reveals a site-selective attachment: The spherical C_{60} units are almost exclusively (94% out of >700 molecules) centered above the upper porphyrin of the $Ce(TPP)_2$ complex, regardless of the orientation (α or β) of the subjacent unit (cf. Figure 1c). We can rule out an embedding of C_{60} in the $Ce(TPP)_2$ arrays since the C_{60} could be selectively removed by STM manipulation revealing an unaltered double-decker species underneath. In addition, the apparent height of C_{60} measured with respect to the double decker is 8.6 Å (at V_b = 1.8 V), considerably higher than for C_{60} directly adsorbed on the metal (7 Å), indicating an electronic decoupling (vide infra), thereby confirming the adsorption of the acceptor on the $Ce(TPP)_2$. Thus, the C_{60} follows the square lattice of the underlying double-decker array (cf. Figure 1e) resulting in a minimal interfullerene distance of 13.9 Å clearly exceeding typical C_{60} nearest-neighbor distances of ~10 Å on bare metal (vide infra).

Several recent studies applied surface templated nanostructures for the organization of fullerenes, including porphyrins and various other species as steering agents.[32−39] Solid-state architectures and assemblies in solution reveal a general attractive interaction between porphyrins and fullerenes, resulting in structures characterized by fullerenes in close face-to-face contact to the porphyrin macrocycle.[7,8] It is generally agreed that these supramolecular complexes are stabilized by noncovalent bonding between the π-systems combined with electrostatic interactions and charge transfer. However, these attractive interactions proved generally insufficient to guide the positioning of C_{60} following deposition on generic 2D porphyrin arrays supported on metallic surfaces.[32] Instead of binding to the porphyrin macrocycle, the fullerene species tend to incorporate into mixed porphyrin–C_{60} arrays, maximizing the C_{60}–metal interaction and thus hampering the prospects outlined in the introduction.[27,28,40−42] In ultrahigh vacuum, the confinement of C_{60} on a tetrapyrrolic macrocycle was achieved partially by employing a phthalocyanine derivative substituted by bulky terminal groups.[43] Even at solid–liquid interfaces, a face-to-face adsorption of fullerenes on porphyrins is uncommon and was only accomplished by employing open-cage C_{60} derivatives,[44,45] whereas an off-center adsorption of C_{60} was possible on a mixed molecular template.[46]

Here we present a genuine site-selective molecular recognition in a solvent-free environment where the C_{60} species are positioned on the π-conjugated upper porphyrin core of the double-decker complex, thus permitting a direct electronic interaction between the potential donor and the acceptor units. It is important to stress that the face-to-face bonding motif is thermally robust and persists after annealing at room temperature. Our DFT calculations elucidate the C_{60}–$Ce(TPP)_2$ coupling: Upon binding of the fullerene, the two-fold bowl shape of the $Ce(TPP)_2$ prevails and the phenyl groups of the top porphyrin tilt slightly away from the C_{60} (cf. Figure 1d). The resulting binding energy for C_{60} exposing a 6:6 bond to the center of the top porphyrin (vide infra) amounts to 1.16 eV and is mainly given by dispersion, i.e., van der Waals interaction. Only minor polarization effects contribute to the binding (cf. Figure S3, Supporting Information). The calculations confirm that the peculiar concave deformation of the top porphyrin maximizes the π–π interaction with the convex surface of the C_{60} and promotes the site-selective adsorption and the successful formation of a surface anchored C_{60}–porphyrin dyad. Related shape-complementarity features were recently employed to stabilize fullerenes on corranulene bowls on Cu(110).[47,48]

The electronic structure of the C_{60}–$Ce(TPP)_2$ dyad was characterized by recording differential conductance spectra above the center of the complex. Figure 2 compares a typical dI/dV spectrum of a C_{60} on top of a double-decker complex (red curve) to reference signals recorded on an individual C_{60} molecule in direct contact with the Ag(111) surface (green curve) and a bare $Ce(TPP)_2$ complex (black curve), respectively.

dx.doi.org/10.1021/nl301534p | Nano Lett. XXXX, XXX, XXX–XXX

As we reported recently,[14] the spectrum of the bare $Ce(TPP)_2$ unit is dominated by a strong resonance at 1.8 eV. The first feature in the positive region (unoccupied state) is observed at 1.1 eV and in the occupied region at around −1.2 eV, yielding an apparent gap of ∼2.3 eV.

The reference spectrum of individual C_{60} molecules on Ag(111) shows two prominent unoccupied resonances [lowest unoccupied molecular orbital (LUMO) at 0.5 eV and LUMO +1 at 1.8 eV, respectively] and a highest occupied molecular orbital (HOMO) close to −1.9 eV, exhibiting a band gap of 2.4 eV. Considering screening shifts, the energetic positions of these frontier orbitals agree well with (inverse) photoemission data of a monolayer of C_{60}−Ag(111)[49] and with our spectra taken on an island of C_{60}−Ag(111).

Addressing now the spectrum recorded above the C_{60} molecule adsorbed on $Ce(TPP)_2$, drastic modifications are observed. Three specific features evidence a considerable reduction of the coupling of the fullerenes with the metallic substrate mediated by the $Ce(TPP)_2$: (i) A sharp spectral feature appears at 1.4 eV in the positive region and is associated with the C_{60} LUMO (see below). However no HOMO signature could be detected in the accessible bias voltage range, suggesting that the HOMO resonance is shifted below −2.5 eV. The sharpening of the LUMO resonance combined with the increase of the band gap to a value exceeding 3.9 eV indicates a reduced electronic coupling to the surface.[50] Previous studies have shown the electronic bandgap of a free C_{60} to be 4.9 eV,[51] whereas the gap of a C_{60} weakly coupled to a substrate amounts to 3.5 eV.[50,52] In our scenario, the screening by image charges in the substrate is reduced, which leads to a larger on-site Hubbard energy due to a higher Coulomb repulsion resulting in an increase of the gap which is apparently not compensated by polarization screening induced in the porphyrin complex.[49,51] (ii) We see additional sidebands separated from the main LUMO and LUMO+1 resonances of the C_{60} (not shown), identifying a free molecule character subject to the dynamic Jahn−Teller effect.[50] (iii) We find a pronounced negative differential resistance (NDR) regime on the high-energy side of the LUMO resonance (1.8−2.7 eV, cf. Figure 2) characteristic for molecular systems exhibiting only weak interactions with the substrate.[53,54] Thus, we tentatively consider these spectral features as a fingerprint of a nearly free-molecule character. It should be noted that the STM tip was characterized before and after all dI/dV and $I(t)$ measurements to exclude the influence of tip modifications: No change in topographic images was detected, which rules out a C_{60} transfer to the tip. In addition, reference spectra on Ag(111) did not reveal any modification before and after the spectra on the molecular system, thereby ensuring an unaltered electronic configuration of the tip.

Our results suggest a potential use of the D−A $Ce(TPP)_2$−C_{60} units in photophysical devices for the following reasons: (i) The double-decker species presents an apparent energy gap of 2.3 eV (540 nm), which suggests a feasible adsorption of light in the visible range in order to generate excitons, provided the transition is dipole-allowed. (ii) The spectra of the double decker indicate a reduced coupling with the metallic substrate, which enhances the lifetime of the excitons.

High-resolution STM images reveal information on the precise orientation of the C_{60} cage in space. Addressing first the reference case of C_{60}−Ag(111) after dosage at 120 K, the majority of C_{60} units do not appear as perfect spheres but exhibit three characteristic lobes when the unoccupied states are probed (cf. Figure 3a). This appearance is well-known to represent the three-fold symmetric shape of the LUMO mainly localized on the pentagonal rings when a fullerene adsorbs with a hexagon facing the substrate.[55−57] Submolecular resolved STM images probing the unoccupied states reveal specific orientations of the C_{60} species centered on $Ce(TPP)_2$, differing from C_{60}−Ag(111). For each orientation of the top porphyrin (α or β), three different orientations of the C_{60} can be distinguished (cf. Figure 3b), giving a total number of six orientations represented by double protrusions symmetric with respect to surface normal and single protrusions appearing off-center, respectively (cf. Figure 3c,d). Again, these intramolecular features stem from the LUMO states of the fullerene mainly residing on the C_{60} pentagons.[58] By comparing STM images and extended Hückel theory (EHT) simulations based on various orientations of an isolated C_{60} cage,[33] we conclude that C_{60} exposes either a C−C bond at the 6:6 ring juncture (labeled 6:6 bond, cf. Figure 3c,d top panel) or an apex atom (cf. Figure 3c,d middle and bottom panel) to the porphyrin center (and thus to vacuum). As summarized in Figure 3, the 6:6 bond configurations correspond to the double protrusions in the STM images, and the apex adsorption yields the off-center protrusion. The excellent agreement between the EHT calculation based on the LUMO charge density of a free C_{60} with the experimental STM topographs recorded at voltages above 1.4 V confirms the identification of the unoccupied spectral feature in the C_{60}−$Ce(TPP)_2$ spectrum with the fully degenerate LUMO (cf. Figure 2a).

Clearly, the macrocycle deformation accounting for the α or β species guides the C_{60} adsorption on the $Ce(TPP)_2$. The 6:6 bond is aligned with the main axis of the top porphyrin, yielding orientations differing by 90° for α and β units, respectively. Analogously, the pentagon corresponding to the apex atom can be displaced to either side of the main axis for both α and β species, resulting in four distinct configurations to be named apex α_1 (β_1) and apex α_2 (β_2). A detailed statistical analysis shows a population of 22.1 ± 3% for the α_1 orientation, 21.7 ± 3% for β_1, 20.9 ± 3% for α_2 and β_2, and 14.3 ± 3% for the 6:6 orientation (identically populated on both orientations of the double decker). Thus, all apex configurations are equiprobable and show a slight statistical preference over the 6:6 orientations. In porphyrin−fullerene crystal structures, a close alignment of a 6:6 bond with a trans N···N vector and therefore the main axis of the porphyrin macrocycle is a well-established structural motif guiding the supramolecular interactions.[8,21,59] For the C_{60}−$Ce(TPP)_2$ dyad, this 6:6 bond adsorption geometry is regularly observed but judging from the above statistics is energetically less favored than the apex configurations.

By comparison, the DFT calculations yield a binding energy of 1.16 eV for the 6:6 configuration and 1.09 eV for the apex orientation. Hence there is a rather small energy difference between the two observed configurations, when modeled as isolated species. Even though the DFT results do not include the presence of the metallic substrate and are restricted to a fixed macrocycle alignement, the computational modeling results thus qualitatively agree with the experimentally verified coexistence of both configurations. The distinct bonding configurations of C_{60} on the porphyrin double deckers signal an interaction sensitive to the nonuniform charge distribution in both entities, as pointed out earlier,[21] and with the present system additionally reflecting the symmetry and distortion of the upper porphyrin ligand.

dx.doi.org/10.1021/nl301534p | Nano Lett. XXXX, XXX, XXX−XXX

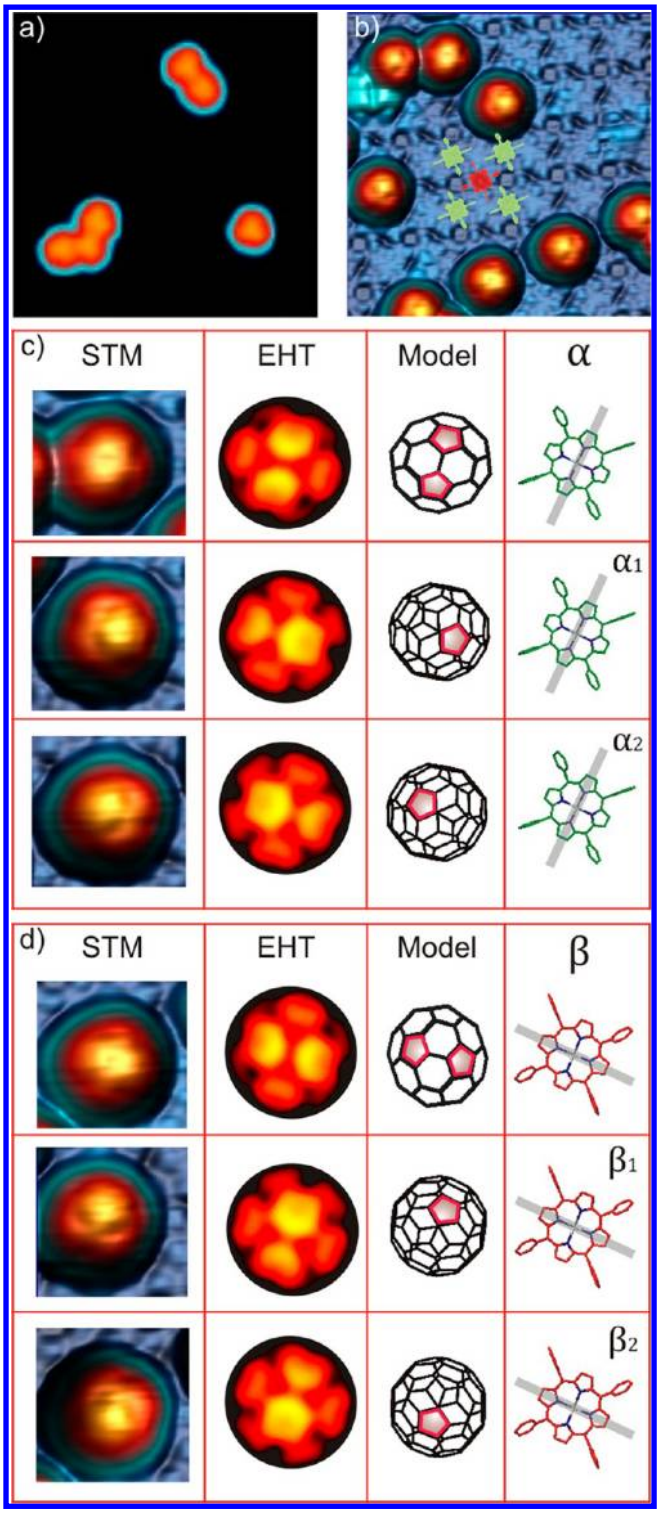

Figure 3. C_{60} orientations on $Ce(TPP)_2$. (a) On Ag(111), the C_{60} molecules expose a hexagon to the substrate and are thus visualized with a three-lobe structure when the unoccupied states are probed. Image size: 110.7 × 110.7 Å^2, V_b = 1.7 V, I = 0.1 nA. (b) A pseudo 3D view of an STM image of C_{60} on $Ce(TPP)_2$ showing distinct orientations of the C_{60} units on the double-decker array. A model of the $Ce(TPP)_2$ unit cell is superimposed, depicting the α (green) and β orientation (red) of the top porphyrin moiety, respectively. Image size: 110.7 × 110.7 Å^2, V_b = 1.8 V, I = 70 pA. (c) The first column shows STM images of the three possible orientations of the C_{60} on an α-$Ce(TPP)_2$ complex. The middle column represents EHT simulations of the LUMO of C_{60} oriented to match the STM image (see text for discussion). The third column schematically shows the C_{60} orientation according to the experimental and simulated images and relates it to the symmetry axis of the α-$Ce(TPP)_2$ (shown in the fourth column). (d) Analogy to (c) but displaying the C_{60} on a β-$Ce(TPP)_2$ complex (rotated 90° with respect to the α-$Ce(TPP)_2$ species).

The stereochemical interaction of the C_{60} cage with the porphyrin macrocycle results in preferred geometrical alignments within the C_{60}–$Ce(TPP)_2$ dyad, i.e., the intermolecular coupling is guided by the relative orientation of the two constituents. Controlling the orientation of the C_{60} cage on the double decker opens the opportunity to tune the coupling in the dyad. Therefore, we now address the deliberate rotation of C_{60} on $Ce(TPP)_2$ via controlled stimulation using an atomically sharp STM tip.

A tunneling current applying a positive sample voltage exceeding a threshold of 1.8 V drives reversible switching between any of the previously discussed C_{60} orientations (cf. Figure 4a). Below this bias threshold, the C_{60}–$Ce(TPP)_2$ dyad can be imaged stably, guaranteeing a reliable read-out of the C_{60} orientation. An inspection of the STM images before and after switching reveals that the rocking motion occurs without any detectable lateral[60] translation of the C_{60}, remaining confined at the center of the porphyrin for both α and β species. The dynamic process is not a simple azimuthal rotation of the C_{60} around a symmetry axis perpendicular to the surface but involves a polar angle, i.e., a second rotation axis in the equatorial plane. This free rotation in space is exemplified in the transition from a 6:6 bond to an apex configuration. It can proceed via a rotation by a polar angle of ±77° around an in-plane axis aligned with the main axis of the porphyrin macrocycle (cf. dashed lines in Figures 1b and 3c) or by a combination of polar and azimuthal angles.

To gain further insight into the rocking process,[61] we record the tunneling current I versus the time t. To this end, the tip is centered above a C_{60}, and the feedback loop is opened. A typical $I(t)$ trace, as displayed in Figure 4b, clearly reveals a switching between three well-separated current levels, representing high, medium, and low conductance states. Within the time resolution of the STM experiment, the transition between the states is abrupt. The absence of such switching events on $Ce(TPP)_2$ arrays demonstrate that the effect is related to C_{60}. By comparing the initial and final current levels in the $I(t)$ traces to STM images recorded before and after many manipulation sequences, we unambiguously can assign the current levels to specific C_{60} orientations. For each porphyrin species (α or β), the high-conductance state represents the apex α_2 (β_2) orientation, the medium conductance state is attributed to the apex configuration α_1 (β_1), while the low conductance state corresponds to the 6:6 bond coupling. Herein, the low-conductance in the 6:6 configuration could originate in a topographic effect given by the central depression observed in the STM images. However, the different current levels for α_1 and α_2 (or β_1 and β_2, respectively), which represent perfectly symmetric configurations when only considering the C_{60} unit, reveal the influence of the C_{60}–$Ce(TPP)_2$ coupling. The asymmetry in the double-decker structure discussed previously (compare Figure S1) seems to influence the electric contacts and thus the coupling in the junction. Indeed, the

dx.doi.org/10.1021/nl301534p | Nano Lett. XXXX, XXX, XXX–XXX

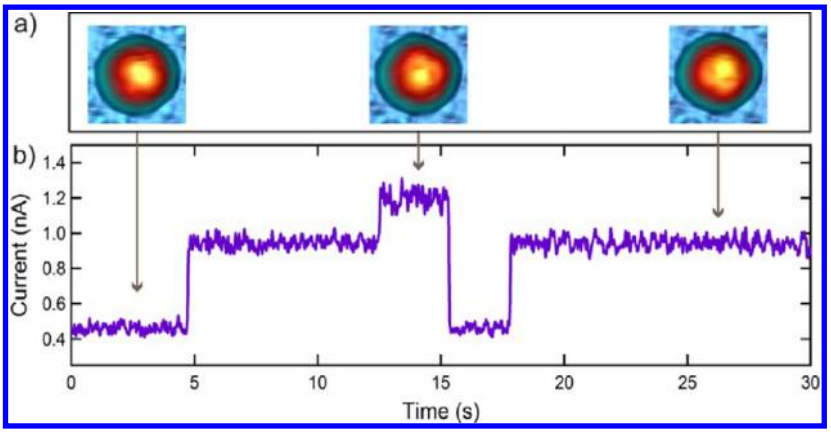

Figure 4. C_{60}–$Ce(TPP)_2$ dyad as a electronic tristable system. (a) Orientational switching of C_{60} adsorbed on an β-$Ce(TPP)_2$ complex. The STM images represent three configurations of the very same C_{60} molecule. (b) Tunneling current measured versus time above a C_{60}–$Ce(TPP)_2$ complex under open feedback loop at 2.2 V. Three different levels of conductance are distinguished: each level is attributed to one orientation of the C_{60}. The highest level of conductance is assigned to an β_2 apex orientation, the adjacent one to the β_1 apex configuration and the lowest level of conductance represents the 6:6 bond orientation.

configurations exhibiting a high and medium conductance (α_2, β_2 and α_1, β_1, respectively) are observed more frequently than the 6:6 state with the lowest conductance.

Thus, the C_{60} on $Ce(TPP)_2$ behaves as a tristable system controllable by STM manipulation. The induced rotations of the C_{60} cage in space affect the intradyad coupling. Consequently, these results unambigously demonstrate deliberate reversible modifications within a surface anchored van der Waals complex.

In summary, we have studied the structural characteristics and the electronic properties of a van der Waals D–A dyad accessing the single molecule level using C_{60}–$Ce(TPP)_2$ on Ag(111) as a model system. C_{60} binds site-selectively face-to-face above the center of the $Ce(TPP)_2$ complexes implying a molecular recognition process, favored by a nonplanar deformation of the top porphyrin, which fits to the convex shape of C_{60}. DFT calculations evidence a bowl-shaped top porphyrin of the $Ce(TPP)_2$ that confines the C_{60}. The C_{60} exhibits a total of three distinct orientations per double-decker species, which are identified by a comparison of STM data to extended Hückel simulations. These well-defined configurations evidence specific stereochemical interactions between the fullerene and the porphyrin guiding the intradyad coupling. By stimulation with the STM tip, individual C_{60} units can be switched reversibly between the three orientations, each revealing a unique level of conductance. Comparative scanning tunneling spectra show that the $Ce(TPP)_2$ strongly reduces the coupling of the C_{60} to the metallic substrate: The band gap increases, and an NDR region emerges. This decoupling from a metallic support is a prerequisite for potential charge separation in the D–A complex under optical excitation. Altogether, C_{60}–$Ce(TPP)_2$ is a promising model system for a noncovalently stacked molecular interface, where even the intradyad coupling can be varied in a controlled way.

■ ASSOCIATED CONTENT

Supporting Information

Additional information and figures. This material is available free of charge via the Internet at http://pubs.acs.org.

■ AUTHOR INFORMATION

Corresponding Author

*E-mail: wilhelm.auwaerter@ph.tum.de; david.ecija.fernandez@ph.tum.de

Notes

The authors declare no competing financial interest.

■ ACKNOWLEDGMENTS

We thank Felix Bischoff for fruitful discussions. Work supported by the ERC Advanced Grant MolArt (no. 247299), the German Research Foundation (DFG) through BA 3395/2-1, the TUM-IAS, and the Munich Center for Advanced Photonics (MAP).

■ REFERENCES

(1) Tang, C. W. *Appl. Phys. Lett.* **1986**, *48* (2), 183–185.
(2) Yu, G.; Gao, J.; Hummelen, J. C.; Wudl, F.; Heeger, A. J. *Science* **1995**, *270* (5243), 1789–1791.
(3) Yang, F.; Shtein, M.; Forrest, S. R. *Nat. Mater.* **2005**, *4*, 37–41.
(4) Günes, S.; Neugebauer, H.; Sariciftci, N. S. *Chem. Rev.* **2007**, *107* (4), 1324–1338.
(5) Roncali, J. *Acc. Chem. Res.* **2009**, *42* (11), 1719–1730.
(6) Heremans, P.; Cheyns, D.; Rand, B. P. *Acc. Chem. Res.* **2009**, *42* (11), 1740–1747.
(7) Guldi, D. M. *Chem. Soc. Rev.* **2002**, *31*, 22–36.
(8) Boyd, P. D. W.; Reed, C. A. *Acc. Chem. Res.* **2005**, *38*, 235–242.
(9) Martín, N.; Sánchez, L.; Illescas, B.; Pérez, I. *Chem. Rev.* **1998**, *98* (7), 2527–2548.
(10) Chen, Y.; Su, W.; Bai, M.; Jiang, J.; Li, X.; Liu, Y.; Wang, L.; Wang, S. *J. Am. Chem. Soc.* **2005**, *127* (45), 15700–15701.
(11) Ishikawa, N.; Sugita, M.; Ishikawa, T.; Koshihara, S.; Kaizu, Y. *J. Am. Chem. Soc.* **2003**, *125*, 8694–8695.
(12) Liu, Z.; Yasseri, A. A.; Lindsey, J. S.; Bocian, D. F. *Science* **2003**, *302* (5650), 1543–1545.
(13) Shinkai, S.; Ikeda, M.; Sugasaki, A.; Takeuchi, M. *Acc. Chem. Res.* **2001**, *34*, 494–503.
(14) Écija, D.; Auwärter, W.; Vijayaraghavan, S.; Seufert, K.; Bischoff, F.; Tashiro, K.; Barth, J. V. *Angew. Chem., Int. Ed.* **2011**, *50* (17), 3872–3877.
(15) Ng, D. K. P.; Jiang, J. *Chem. Soc. Rev.* **1997**, *26* (6), 433–442.
(16) Jiang, J.; Ng, D. K. P. *Acc. Chem. Res.* **2008**, *42* (1), 79–88.
(17) Li, Y.; Bian, Y.; Yan, M.; Thapaliya, P. S.; Johns, D.; Yan, X.; Galipeau, D.; Jiang, J. *J. Mater. Chem.* **2011**, *21* (30), 11131–11141.

(18) Wang, Q.; Li, Y.; Yan, X.; Rathi, M.; Ropp, M.; Galipeau, D.; Jiang, J. *Appl. Phys. Lett.* **2008**, *93* (7), 073303.
(19) Liu, M. O.; Hu, A. T. *J. Organomet. Chem.* **2004**, *689* (15), 2450−2455.
(20) Liu, M. O.; Hu, A. T. *J. Porphyrins Phthalocyanines* **2003**, *7* (9), 565.
(21) Wang, Y.-B.; Lin, Z. *J. Am. Chem. Soc.* **2003**, *125*, 6072−6073.
(22) Boyd, P. D. W.; Hodgson, M. C.; Rickard, C. E. F.; Oliver, A. G.; Chaker, L.; Brothers, P. J.; Bolskar, R. D.; Tham, F. S.; Reed, C. A. *J. Am. Chem. Soc.* **1999**, *121* (45), 10487−10495.
(23) Liao, M.-S.; Watts, J. D.; Huang, M.-J. *J. Phys. Chem. B* **2007**, *111*, 17.
(24) Thompson, B. C.; Fréchet, J. M. J. *Angew. Chem., Int. Ed.* **2008**, *47* (1), 58−77.
(25) Ballesteros, B.; de la Torre, G.; Shearer, A.; Hausmann, A.; Herranz, M. Á.; Guldi, D. M.; Torres, T. *Chem.—Eur. J.* **2010**, *16* (1), 114−125.
(26) Guldi, D. M.; Gouloumis, A.; Vázquez, P.; Torres, T.; Georgakilas, V.; Prato, M. *J. Am. Chem. Soc.* **2005**, *127* (16), 5811−5813.
(27) Sedona, F.; Di Marino, M.; Sambi, M.; Carofiglio, T.; Lubian, E.; Casarin, M.; Tondello, E. *ACS Nano* **2010**, *4* (9), 5147−5154.
(28) Kiebele, A.; Bonifazi, D.; Cheng, F.; Stöhr, M.; Diederich, F.; Jung, T.; Spillmann, H. *ChemPhysChem* **2006**, *7* (7), 1462−1470.
(29) Barth, J. V. *Annu. Rev. Phys. Chem.* **2007**, *58*, 375−407.
(30) Buchler, J. W.; De Cian, A.; Fischer, J.; Kihn-Botulinski, M.; Paulus, H.; Weiss, R. *J. Am. Chem. Soc.* **1986**, *108* (13), 3652−3659.
(31) Liao, M.-S.; Watts, J. D.; Huang, M.-J. *J. Phys. Chem. A* **2006**, *110* (48), 13089−13098.
(32) Sánchez, L.; Otero, R.; Gallego, J. M.; Miranda, R.; Martin, N. *Chem. Rev.* **2009**, *109*, 2081−2091.
(33) Ait-Mansour, K.; Ruffieux, P.; Gröning, P.; Fasel, R.; Gröning, O. *J. Phys. Chem. C* **2009**, *113*, 5292−5299.
(34) Theobald, J. A.; Oxtoby, N. S.; Phillips, M. A.; Champness, N. R.; Beton, P. H. *Nature* **2003**, *424*, 1029−1031.
(35) Stepanow, S.; Lingenfelder, M.; Dmitriev, A.; Spillmann, H.; Delvigne, E.; Lin, N.; Deng, X.; Cai, C.; Barth, J. V.; Kern, K. *Nat. Mat.* **2004**, *3*, 229−233.
(36) Stepanow, S.; Lin, N.; Barth, J. V.; Kern, K. *Chem. Commun.* **2006**, 2153−2155.
(37) Mena-Osteritz, E.; Bäuerle, P. *Adv. Mater.* **2006**, *18*, 447−451.
(38) Pan, G.-B.; Liu, J.-M.; Zhang, H.-M.; Wan, L.-J.; Zheng, Q.-Y.; Bai, C.-L. *Angew. Chem. Int. Ed* **2003**, *42* (24), 2747−2751.
(39) Silly, F.; Shaw, A. Q.; Porfyrakis, K.; Briggs, G. A. D.; Castell, M. R. *Appl. Phys. Lett.* **2007**, *91* (25), 253109.
(40) Bonifazi, D.; Spillmann, H.; Kiebele, A.; de Wild, M.; Seiler, P.; Cheng, F.; Güntherodt, H.-J.; Jung, T.; Diederich, F. *Angew. Chem., Int. Ed.* **2004**, *43* (36), 4759−4763.
(41) Di Marino, M.; Sedona, F.; Sambi, M.; Carofiglio, T.; Lubian, E.; Casarin, M.; Tondello, E. *Langmuir* **2009**, *26* (4), 2466−2472.
(42) Nishiyama, F.; Yokoyama, T.; Kamikado, T.; Yokoyama, S.; Mashiko, S.; Sakaguchi, K.; Kikuchi, K. *Adv. Mater.* **2007**, *19* (1), 117−120.
(43) Samuely, T.; Liu, S.-X.; Haas, M.; Decurtins, S.; Jung, T. A.; Stöhr, M. *J. Phys. Chem. C* **2009**, *113* (45), 19373−19375.
(44) Yoshimoto, S.; Tsutsumi, E.; Honda, Y.; Murata, Y.; Murata, M.; Komatsu, K.; Ito, O.; Itaya, K. *Angew. Chem., Int. Ed.* **2004**, *116*, 3106−3109.
(45) Yoshimoto, S.; Honda, Y.; Murata, Y.; Murata, M.; Komatsu, K.; Ito, O.; Itaya, K. *J. Phys. Chem. B* **2005**, *109* (18), 8547−8550.
(46) Yoshimoto, S.; Honda, Y.; Ito, O.; Itaya, K. *J. Am. Chem. Soc.* **2007**, *130* (3), 1085−1092.
(47) Xiao, W.; Passerone, D.; Ruffieux, P.; Aït-Mansour, K.; Gröning, O.; Tosatti, E.; Siegel, J. S.; Fasel, R. *J. Am. Chem. Soc.* **2008**, *130* (14), 4767−4771.
(48) Bauert, T.; Baldridge, K. K.; Siegel, J. S.; Ernst, K.-H. *Chem. Commun.* **2011**, *47* (28), 7995−7997.
(49) Hesper, R.; Tjeng, L. H.; Sawatzky, G. A. *Europhys. Lett.* **1997**, *40* (2), 177−182.
(50) Frederiksen, T.; Franke, K. J.; Arnau, A.; Schulze, G.; Pascual, J. I.; Lorente, N. *Phys. Rev. B* **2008**, *78*, 233401.
(51) Fernández-Torrente, I.; Franke, K. J.; Pascual, J. I. *J. Phys.: Condens. Matter* **2008**, *20*, 184001.
(52) Cho, J.; Smerdon, J.; Gao, L.; Süzer, Ö.; Guest, J. R.; Guisinger, N. P. *Nano Lett.* **2012**, *12* (6), 3018−3024.
(53) Grobis, M.; Wachowiak, A.; Yamachika, R.; Crommie, M. F. *Appl. Phys. Lett.* **2005**, *86*, 204102.
(54) Franke, K. J.; Schulze, G.; Henningsen, N.; Fernández-Torrente, I.; Pascual, J. I.; Zarwell, S.; Rück-Braun, K.; Cobian, M.; Lorente, N. *Phys. Rev. Lett.* **2008**, *100* (3), 036807.
(55) Sakurai, T.; Wang, X.-D.; Xue, Q. K.; Hasegawa, Y.; Hashizume, T.; Shinohara, H. *Prog. Surf. Sci.* **1996**, *51*, 261−408.
(56) Tamai, A.; Seitsonen, A. P.; Fasel, R.; Shen, Z.-X.; Osterwalder, J.; Greber, T. *Phys. Rev. B* **2005**, *72*, 085421.
(57) Li, H. I.; Pussi, K.; Hanna, K. J.; Wang, L.-L.; Johnson, D. D.; Cheng, H.-P.; Shin, H.; Curtarolo, S.; Moritz, W.; Smerdon, J. A.; McGrath, R.; Diehl, R. D. *Phys. Rev. Lett.* **2009**, *103*, 056101.
(58) Lu, X.; Grobis, M.; Khoo, K. H.; Louie, S. G.; Crommie, M. F. *Phys. Rev. Lett.* **2003**, *90* (9), 096802.
(59) Bhyrappa, P.; Karunanithi, K. *Inorg. Chem.* **2010**, *49*, 8389−8400.
(60) Keeling, D. L.; Humphry, M. J.; Fawcett, R. H. J.; Beton, P. H.; Hobbs, C.; Kantorovich., L. *Phys. Rev. Lett.* **2005**, *94* (14), 146104.
(61) Muntwiler, M.; Auwärter, W.; Seitsonen, A. P.; Osterwalder, J.; Greber, T. *Phys. Rev. B* **2005**, *71* (12), 121402.

dx.doi.org/10.1021/nl301534p | *Nano Lett.* XXXX, XXX, XXX−XXX